

The quantum square-well fluid: a thermodynamic geometric view

J. L. López-Picón,^{1,*} L. F. Escamilla-Herrera,^{1,†} Alejandro Gil-Villegas,^{1,‡} and José Torres-Arenas^{1,2,§}

¹*División de Ciencias e Ingenierías Campus León, Universidad de Guanajuato,
A.P. E-143, C.P. 37150, León, Guanajuato, México.*

²*Departamento de Física Aplicada, Universidade de Vigo, Spain*

(Dated: March 10, 2026)

We investigate several aspects of the thermodynamic geometry for a quantum fluid with square-well interactions using a third-order perturbation-theory framework based on the path-integral-necklace analogy. A comparison is made between the thermodynamic and geometric properties of the quantum fluid and its classical counterpart for the interaction ranges $\lambda^* = 1.3, 1.5,$ and 1.7 . In particular, we analyze the scalar-curvature behavior, criticality, and the corresponding Widom lines derived from curvature and several thermodynamic response functions. Quantum effects are shown to smooth supercritical anomalies of the scalar curvature and to shift its extrema for short-range interactions, while leaving the critical exponents of both the curvature and its heat capacity consistent with mean-field predictions. Widom lines associated with temperature-dependent response functions and with the curvature scalar exhibit pronounced classical-quantum differences for short interaction ranges; in contrast, those derived from the isothermal compressibility exhibit only minor variations. Overall, these results highlight the sensitivity of geometric information of thermodynamic systems due to quantum effects and the crucial role of the interaction range in shaping supercritical thermodynamic behavior.

PACS numbers: 05.20.Jj, 95.30.Sf, 95.30.Tg

Keywords: Statistical Mechanics, Square-well fluid, Thermodynamic Geometry

I. INTRODUCTION

For certain substances such as hydrogen, deuterium, helium and neon, it has been well known for decades that it is necessary to consider quantum contributions to model the behavior of the molecules to accurately predict their thermodynamic and structural properties [1–14]. For the sake of simplicity, throughout this work we will refer to fluids exhibiting these features as *quantum fluids*.

Quantum fluids represent a distinctive class of systems in which atomic or molecular motion cannot be accurately described within a classical framework. Even when effective pairwise additive potentials are employed to model electrostatic interactions, nuclear motion must still be treated from a non-classical framework.

Quantum effects become significant when the thermal de Broglie wavelength, $\lambda_B = h/\sqrt{2m\pi k_B T}$ (where h is the Planck constant, k_B the Boltzmann constant, m the particle mass and T stands for temperature), is comparable to the characteristic interparticle spacing, thereby the classical description in such cases is inadequate. This regime becomes particularly relevant for substances with low-mass particles, such as those found in hydrogen, deuterium, helium, and neon, where phenomena such as zero-point motion and quantum tunneling could play a dominant role [15, 16].

Quantum fluids offer practical applications in areas such

as energy storage and cryogenic transport. Such systems provide a valuable testing ground for exploring quantum effects in dense, interacting media and contribute to a deeper understanding of matter under extreme thermodynamic conditions [17, 18].

The study of quantum fluids has progressed through both theoretical analyzes and computational simulations. A variety of frameworks have been formulated to characterize these systems, including perturbation theory, Gaussian wave packets, quantum Monte Carlo techniques, and the path integral (PI) formalism [2, 10–12, 19–26].

One possible route to obtain quantum predictions in thermodynamic systems involves introducing corrections to classical expressions. Under this approach, many of the seminal works exploring the thermodynamic properties of systems with quantum considerations used semiclassical approximations [27–29].

In early efforts to model quantum systems, the hard sphere model has played a very important role, first as an individual quantum fluid system but also in its role as a reference system in perturbation theories [1, 19, 24, 30–33]. On the other hand, the Feynman–Hibbs path-integral method represents each particle as a polymer-like ring composed of classical beads connected by harmonic springs. The corresponding path integrals can be evaluated using Monte Carlo, molecular dynamics, or Brownian dynamics techniques. This technique allows to obtain precise quantum description of the studied systems.

In recent years, the Feynman–Hibbs path-integral method, thermodynamic perturbation theory and the SAFT-VR approach [34] have been successfully applied to the quantum Square-Well (SW) fluid [24], one of the simplest yet most informative models in Statistical Mechanics. Defined by a hard-core repulsion and a finite-

*Electronic address: lopezjl@ugto.mx

†Electronic address: lf.escamilla@ugto.mx

‡Electronic address: gil@fisica.ugto.mx

§Electronic address: jtorres@fisica.ugto.mx

range attractive well, the SW potential captures essential features of intermolecular interactions while remaining analytically and computationally tractable. Its piecewise definition allows for a clear separation between repulsive and attractive contributions, making it an ideal framework for assessing theoretical developments and exploring phase behavior. Consequently, the SW fluid has been extensively used to study liquid–gas coexistence, critical phenomena, and the thermodynamic properties of simple and associating fluids [34–40]. In the present study, we employ a Helmholtz free energy expression formulated for the SW fluid, derived within the framework of perturbation theory to explore the thermodynamic geometry of a quantum square-well fluid. The analysis extends the perturbation expansion up to third-order, with the quantum hard-sphere system serving as the reference system and quantum corrections explicitly included in the higher-order contributions.

The quantum fluid under consideration consists of N hard spheres of diameter σ and mass m that interact via a square-well potential of depth ϵ and range λ ,

$$\phi(r) = \begin{cases} \infty, & r < \sigma, \\ -\epsilon, & \sigma \leq r \leq \lambda\sigma, \\ 0, & r > \lambda\sigma. \end{cases} \quad (1)$$

The aforementioned equation of state (EOS) was computed using thermodynamic perturbation theory up to the third-order, according to a Zwanzig expansion in $\beta = 1/k_B T$ [41],

$$\frac{A}{Nk_B T} = \frac{A^{\text{ideal}}}{Nk_B T} + \frac{A^{\text{QHS}}}{Nk_B T} + a_{1PI}\beta + a_{2PI}\beta^2 + a_{3PI}\beta^3. \quad (2)$$

where N is the number of particles, A and A^{QHS} are the Helmholtz free energies of the quantum fluid and the Quantum Hard Sphere (QHS) reference system, respectively; A^{ideal} is the ideal contribution, and a_{nPI} , the perturbation terms. The QHS structural properties required for the evaluation of the perturbation terms were obtained from MC simulations using the exact analogy between the discretized path-integral formulation of quantum mechanics and the partition function of a fluid composed of ring molecules [42]. The SW parameters ϵ and σ are used to define the reduced variables of temperature, $T^* = k_B T/\epsilon$, pressure, $P^* = P\sigma^3/\epsilon$, packing fraction $\eta = \pi\sigma^3\rho/6$, potential range, $\lambda^* = \sigma\lambda$, and the de Boer parameter Λ ,

$$\Lambda = \frac{h}{\sigma\sqrt{m\epsilon}}; \quad (3)$$

In this work, we will set this parameter to $\Lambda = \sqrt{2\pi}/4$, which is close to the value of neon (Ne). We investigate the influence of quantum effects on the thermodynamic geometry of the square-well fluid. This is achieved through a comparative analysis with the corresponding classical system.

This work is organized as follows. In Section II, theoretical expressions of thermodynamic geometry are briefly reviewed, and present the classical and quantum equations of state for the SW system considered in this work. Section III presents the results of our analysis for both the subcritical and supercritical regimes, emphasizing the key differences identified between them highlighting the construction of Widom lines; additionally, critical exponents for all response functions and curvature scalar R are calculated, presented and discussed. Section IV concludes with a summary of the main findings of this work.

II. THEORETICAL METHODS

A. Thermodynamic Geometry

This work is based on the theoretical framework of thermodynamic geometry (TG) developed by G. Ruppeiner [43, 44], which is derived from entropic representation and Einstein-Landau thermodynamic fluctuation theory [45, 46]. This framework is similar to the one previously constructed by Weinhold in energy representation [47]. Although the derived TG metric on the thermodynamic equilibrium space is naturally a metric in entropic representation, it is much more common and convenient to transform this metric into the Helmholtz free energy A representation due to its particular simplicity, because for this potential the metric $[g_{ij}]_A$ becomes diagonal. In terms of energy divided by volume $f = A/V$, the metric is simply,

$$[g_{ij}]_A = \frac{1}{k_B T} \begin{pmatrix} -\frac{\partial^2 f}{\partial T^2} & 0 \\ 0 & \frac{\partial^2 f}{\partial \rho^2} \end{pmatrix}; \quad (4)$$

or, equivalently, in terms of response functions,

$$[g_{ij}]_A = \frac{1}{k_B} \begin{pmatrix} \frac{c_V}{T^2} & 0 \\ 0 & \frac{1}{T\rho^2\kappa_T} \end{pmatrix},$$

where c_V is the constant-volume heat capacity per unit volume, $\rho = N/V$ is the number density, and κ_T is the isothermal compressibility.

For systems written in terms of other thermodynamic potentials with two thermodynamic coordinates $\{X, Y\}$ (a two-dimensional manifold), the scalar curvature R associated with an arbitrary metric g_{ij} not necessarily diagonal, has the general form:

$$R = -\frac{1}{\sqrt{g}} \frac{\partial}{\partial X} \left(\frac{g_{XY}}{g_{XX}\sqrt{g}} \frac{\partial g_{XX}}{\partial Y} - \frac{1}{\sqrt{g}} \frac{\partial g_{YY}}{\partial X} \right) - \frac{1}{\sqrt{g}} \frac{\partial}{\partial Y} \left(\frac{2}{\sqrt{g}} \frac{\partial g_{XY}}{\partial X} - \frac{1}{\sqrt{g}} \frac{\partial g_{XX}}{\partial Y} - \frac{g_{XY}}{g_{XX}\sqrt{g}} \frac{\partial g_{XX}}{\partial X} \right), \quad (5)$$

which simplifies considerably if the metric is diagonal as in eq.4.

Regarding the explicit EOS considered in this work, the function f can be written in terms of the thermodynamic

function $a = \frac{A}{Nk_B T}$,

$$f = \rho k_B T a. \quad (6)$$

For simplicity, in the following, all thermodynamic and geometric quantities are expressed in terms of the reduced set of variables T^* and ρ^* . For this particular set, the components of the metric are:

$$g_{TT} = \frac{1}{\sigma^3} \left(-\rho^* \frac{\partial^2 a}{\partial T^{*2}} - \frac{2\rho^*}{T^*} \frac{\partial a}{\partial T^*} \right) = \frac{1}{\sigma^3} G_{TT}(\rho^*, T^*),$$

$$g_{\rho\rho} = \sigma^3 \left(\rho^* \frac{\partial^2 a}{\partial \rho^{*2}} + 2 \frac{\partial a}{\partial \rho^*} \right) = \sigma^3 G_{\rho\rho}(\rho^*, T^*). \quad (7)$$

The scalar curvature has dimensions of cubed distance, and its reduced expression $R^* = R/\sigma^3$ is given by,

$$R^* = \frac{1}{\sqrt{g}} \frac{\partial}{\partial T^*} \left(\frac{1}{\sqrt{g}} \frac{\partial G_{\rho\rho}}{\partial T^*} \right) + \frac{1}{\sqrt{g}} \frac{\partial}{\partial \rho^*} \left(\frac{1}{\sqrt{g}} \frac{\partial G_{TT}}{\partial \rho^*} \right). \quad (8)$$

Finally, to be able to have a straightforward comparison between the thermodynamic quantities reported in Ref. [24], we use the packing fraction η instead of the number density in our calculations.

B. Equations of State

In this work, we consider the Helmholtz free energy for both a classical square-well fluid and its quantum counterpart, which incorporates quantum-mechanical contributions. In both cases, the free energy expressions are obtained via perturbation theory. An important feature of quantum contributions is their explicit dependence on temperature through the de Broglie thermal wavelength λ_B .

1. Classical SW Helmholtz free energy

For the classical SW fluid, the reference properties are obtained from classical Hard Spheres (HS), and the HS free energy is obtained from the Carnahan-Starling (CS) EOS [48],

$$\frac{A^{\text{HS}}}{Nk_B T} = \frac{4\eta - 3\eta^2}{(1 - \eta)^2}. \quad (9)$$

Only first- and second-order perturbative terms are considered, according to the EOS by Patel and coworkers [40]. The first-order correction is given by,

$$\frac{A_1}{Nk_B T} = -4 \left(\frac{\epsilon}{k_B T} \right) (\lambda^{*3} - 1) \eta g^{\text{HS}}(1; \eta_{\text{eff}}), \quad (10)$$

where g^{HS} is the HS contact radial distribution function evaluated at an effective packing fraction η_{eff} ,

$$g^{\text{HS}}(1; \eta_{\text{eff}}) = \frac{1 - \eta_{\text{eff}}/2}{(1 - \eta_{\text{eff}})^3}; \quad \eta_{\text{eff}} = \frac{c_1 \eta + c_2 \eta^2}{(1 + c_3 \eta)^3}; \quad (11)$$

where c_1, c_2 and c_3 are given by the following polynomials,

$$c_1 = -\frac{3.1649}{\lambda^*} + \frac{13.3501}{\lambda^{*2}} - \frac{14.8057}{\lambda^{*3}} + \frac{5.7029}{\lambda^{*4}}, \quad (12)$$

$$c_2 = \frac{43.0042}{\lambda^*} - \frac{191.6623}{\lambda^{*2}} - \frac{273.8968}{\lambda^{*3}} - \frac{128.9334}{\lambda^{*4}},$$

$$c_3 = \frac{65.0419}{\lambda^*} - \frac{266.4627}{\lambda^{*2}} - \frac{361.0431}{\lambda^{*3}} - \frac{162.6996}{\lambda^{*4}}.$$

The second-order perturbation term is expressed as

$$\frac{A_2}{Nk_B T} = \frac{1}{2} \left(\frac{\epsilon}{k_B T} \right) K^{\text{HS}} \eta \frac{\partial}{\partial \eta} \left(\frac{A_1}{Nk_B T} \right), \quad (13)$$

where the CS HS isothermal compressibility K^{HS} is given by [48]

$$K^{\text{HS}} = \frac{(1 - \eta)^4}{1 + 4\eta + 4\eta^2 + 4\eta^3 \eta^4}. \quad (14)$$

2. Quantum SW (QSW) Helmholtz free energy

The QSW Helmholtz free energy is given by Eq.(2), using the quantum equation of state derived by Serna and Gil-Villegas [24]. The expression for A^{QHS} is the same as the CS equation of state, Eq.(9), evaluated at the packing fraction

$$\eta_{QHS} = (1 + d_1 \lambda_B^*) \eta + (d_2 \lambda_B^* + d_3 \lambda_B^{*2}) \eta^2,$$

with $d_1 = 1.6593854484$, $d_2 = -1.0927115150$ and $d_3 = -1.1188233921$.

The corresponding first perturbation term is given by,

$$a_{1\text{PI}} = -4\eta(\lambda_{\text{eff}}^3 - 1)g_{\text{HS}}, \quad (15)$$

where λ_{eff} is an effective range parameter and

$$g_{\text{HS}} = \frac{1 - \eta_{\text{eff}}/2}{(1 - \eta_{\text{eff}})^3}, \quad (16)$$

$$\eta_{\text{eff}} = c_1(\lambda^*)\eta + c_2(\lambda^*)\eta^2 + c_3\eta^3. \quad (17)$$

The effective range λ_{eff} is given by the following expressions:

$$\lambda_{\text{eff}} = q_0 + q_1 \eta + q_2 \eta^2; \quad (18)$$

where,

$$q_0(\lambda^*) = q_{00} + q_{01} \lambda^*, \quad (19)$$

$$q_1(\lambda^*) = q_{10} + q_{11} \lambda^* + q_{12} \lambda^{*2} + q_{13} \lambda^{*3}, \quad (20)$$

$$q_2(\lambda^*) = q_{20} + q_{21} \lambda^* + q_{22} \lambda^{*2} + q_{23} \lambda^{*3}. \quad (21)$$

and,

$$q_{nm}(\lambda_B) = q_{nm0} + q_{nm1} \lambda_B + q_{nm2} \lambda_B^2 + q_{nm3} \lambda_B^3, \quad (22)$$

The coefficients q_{ij} are given in Table I.

| nm | q_{nm0} | q_{nm1} | q_{nm2} | q_{nm3} |
|------|-----------|---------------|----------------|----------------|
| 00 | 0.0 | -0.5207594172 | 0.1376491457 | 0.1619400037 |
| 01 | 1.0 | 0.2085532937 | -0.09789365585 | -0.09331727334 |
| 10 | 0.0 | 27.87555242 | -16.84467685 | 24.12334316 |
| 11 | 0.0 | -61.37020515 | 35.15220145 | -49.99085495 |
| 12 | 0.0 | 43.76848829 | -23.81353044 | 33.33648824 |
| 13 | 0.0 | -9.887151471 | 5.374121467 | -7.222508701 |
| 20 | 0.0 | -175.6647412 | -0.4555948621 | 14.16499116 |
| 21 | 0.0 | 379.0986356 | -60.59299424 | 2.185720582 |
| 22 | 0.0 | -264.2859871 | 83.30714552 | -23.29735407 |
| 23 | 0.0 | 59.32562146 | -27.68449440 | 9.881196243 |

Table I: Parameters of the effective attractive range λ_{eff} used to describe the quantum mean attractive energy in Eq. (22).

The second-order term is given by [49]

$$a_{2\text{PI}} = \frac{1}{2} K_{\text{HS}} Y a_{1\text{PI}}; \quad (23)$$

where,

$$K_{\text{HS}} = \frac{(1-\eta)^4}{1+4\eta+4\eta^2-4\eta^3-\eta^4}, \quad (24)$$

$$Y = \frac{1+\Omega_1\eta+\Omega_2\eta^2+\Omega_3\eta^3+\Omega_4\eta^4}{(1-\eta)^2}, \quad (25)$$

and,

$$\Omega_i = \Omega_{i0} + \Omega_{i1}\lambda_{\text{eff}} + \Omega_{i2}\lambda_{\text{eff}}^2 + \Omega_{i3}\lambda_{\text{eff}}^3; \quad (26)$$

The coefficients Ω_{ij} ($j = 1, 2, 3$) are given in Table II.

| n | Ω_{n0} | Ω_{n1} | Ω_{n2} | Ω_{n3} |
|-----|---------------|---------------|---------------|---------------|
| 1 | -287.2698 | 564.4165 | -360.5291 | 74.58325 |
| 2 | 2374.631 | -4312.958 | 2557.982 | -494.2050 |
| 3 | -605.3505 | -105.1644 | 885.7259 | -360.7473 |
| 4 | -10317.90 | 21338.96 | -14497.67 | 3243.0211 |

Table II: Parameters for the evaluation of the Y function in the generalized compressibility approximation in Eq. (26).

Finally, the third-order perturbation term is

$$a_{3\text{PI}} = \frac{1}{6} K_{\text{HS}}^2 (1 - S\eta) a_{1\text{PI}}; \quad (27)$$

where

$$S = \frac{49\lambda_{\text{eff}}^5 + 49\lambda_{\text{eff}}^4 - 293\lambda_{\text{eff}}^3 - 5\lambda_{\text{eff}}^2 + 211\lambda_{\text{eff}} + 211}{4(\lambda_{\text{eff}}^2 + \lambda_{\text{eff}} + 1)}. \quad (28)$$

Tables III and IV show, respectively, the classical and quantum critical values of temperature, packing fraction, and pressure for specific SW ranges $\lambda^* = 1.3, 1.5, 1.7$, where it is known that both classical and quantum SW EOS are accurate. The critical values were calculated using standard thermodynamic relations using the equations of state already described.

| λ^* | T_{cr}^* | η_{cr} | P_{cr}^* |
|-------------|-------------------|--------------------|-------------------|
| 1.3 | 0.940934 | 0.206423 | 0.160563 |
| 1.5 | 1.32907 | 0.149937 | 0.143413 |
| 1.7 | 1.76812 | 0.125244 | 0.150339 |

Table III: Critical values for different potential ranges of the classical square-well fluid.

| λ^* | T_{cr}^* | η_{cr} | P_{cr}^* |
|-------------|-------------------|--------------------|-------------------|
| 1.3 | 0.639694 | 0.157293 | 0.0791678 |
| 1.5 | 0.983404 | 0.127644 | 0.0796721 |
| 1.7 | 1.4559 | 0.111839 | 0.109786 |

Table IV: Critical values for different potential ranges of the quantum square-well fluid.

Using these EOS, the thermodynamic geometric curvature and its scalar R are calculated for the classical and quantum square-well equations, in order to understand the role that quantum contributions play in the thermodynamic geometry of the square-well system. An analysis of the behavior of the Widom lines of thermodynamic response functions is also given: thermal expansion coefficient α , isothermal compressibility κ_T and heat capacity at constant pressure C_P , as well as the geometric R -Widom line given by the curvature extrema in the supercritical region.

III. RESULTS

To provide a detailed comparison of the thermodynamic geometry exhibited by classical and quantum square-well fluids, we focus on three representative potential ranges, namely $\lambda^* = 1.3, 1.5$, and 1.7 , which allow us to systematically assess the influence of the interaction range on the resulting geometric behavior.

Our EOS have a restricted domain of validity for both density and temperature. With respect to temperature, their validity is limited, especially in the subcritical region. Therefore, we considered a lower temperature limit based on an estimate of the triple point. The triple point temperature of the SW fluid is known to increase with the potential range[50]. The lower limit for temperature considered in this work for the analyzed ranges is: for $\lambda^* = 1.3$, $T_{\text{min}}^* = 0.7$; for $\lambda^* = 1.5$, $T_{\text{min}}^* = 0.5$; and for $\lambda^* = 1.7$, $T_{\text{min}}^* = 0.4$.

Figure 1 presents the classical and quantum isotherms of the reduced scalar curvature R^* at $T/T_c = 1.25$ for the ranges of selected parameters, spanning supercritical states throughout the full density domain. In this regime, quantum effects smoothen the characteristic anomalies present near the critical point and shift the extrema toward lower densities for short-range potentials.

The region of thermodynamic stability can be determined directly from the curvature scalar R . The spinodal curve is obtained from the divergences exhibited by R in the subcritical region, or equivalently from the zeros of its in-

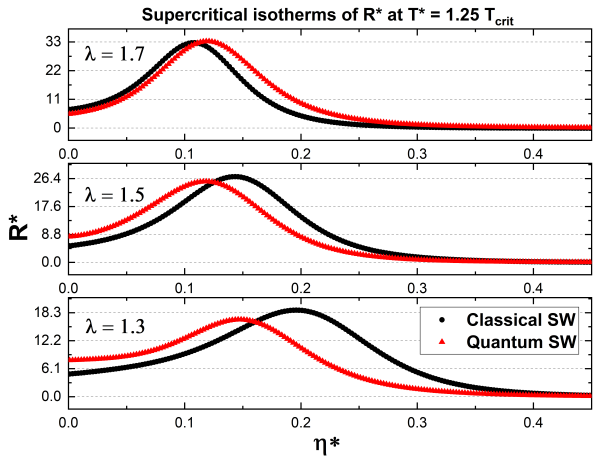


Figure 1: Comparison of the classical and quantum supercritical isotherms of the reduced scalar curvature R^* at a temperature $T^* = 1.25T_c$, for $\lambda^* = 1.3$ (bottom), $\lambda^* = 1.5$ (middle) and $\lambda^* = 1.7$ (top).

verse. Applying this last criteria, the spinodal curves for the interaction ranges studied in this work are presented in Figure 2. As can be observed, quantum effects enlarge the stability region relative to the classical case for short interaction ranges of the potential, tending to converge as the interaction range increases.

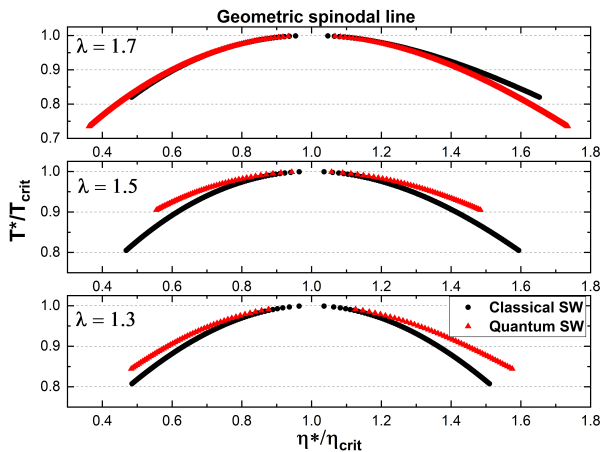


Figure 2: Comparison of the Classical and Quantum geometric spinodal lines for $\lambda^* = 1.3$ (bottom), $\lambda^* = 1.5$ (middle), and $\lambda^* = 1.7$ (upper).

An initial question addressed here is whether the quantum contributions encoded in the free-energy given in Eq. (2) could modify the behavior of the fluid in the vicinity of the critical point. Although such modifications were not anticipated in light of the universality of critical phenomena for fluids, the approximate and perturbative nature of the present theory motivated us to examine this issue explicitly.

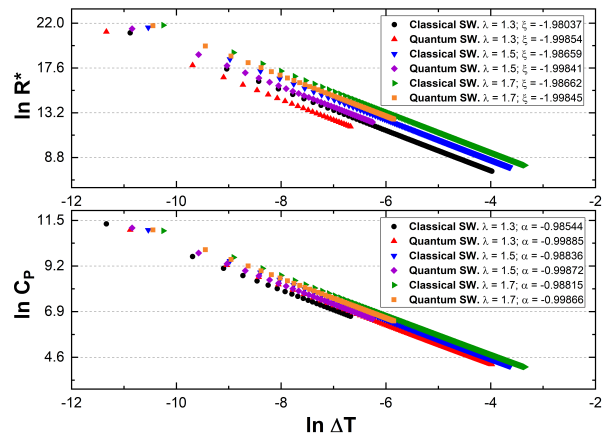


Figure 3: Critical behavior for the classical and quantum square-well curvature R^* (upper) and C_p (bottom). Both quantities are evaluated along the critical isochore ($\eta = \eta_{cr}$), as temperature approaches the critical point from above from 102% to 100.002% its critical value for $\lambda^* = 1.3, 1.5, 1.7$.

As shown in Figure 3, the critical exponents associated to R and C_p for the classical and quantum square-well fluids, are obtained from the expected linear behavior in a log-log plot of the response function versus $\Delta T = T - T_c$ to simplify the numerical approach, reducing computational errors in the iterative process performed. This behavior is obtained via the following relation,

$$\ln [f_{res}(T)] = \beta \ln |\Delta T| + a; \quad (29)$$

where $f_{res}(T)$ stands for the thermodynamic function considered, β is its corresponding critical exponent, and a is the y -intercept, which is an irrelevant offset to the critical behavior of $f_{res}(T)$. This equation is applied approaching from 102% the value of the critical temperature up to 100.002% for $\eta = \eta_{cr}$; we approach the critical point from the supercritical region along the critical isochore. The critical exponents calculated for R^* and C_p , equal to 2 and 1 respectively, are fully consistent with mean-field predictions, in line with the perturbative nature of the theory. Consistently, the results are identical for both the classical and quantum versions of the theory. The behavior near the critical point therefore follows a mean-field description that neglects fluctuations in the thermodynamic variables.

The classical and quantum R -Widom lines are presented in Figure 4. As shown, noticeable differences between the classical and quantum behaviors persist across all ranges considered. Because the scalar curvature involves higher-order derivatives with respect to temperature and density, it is reasonable to attribute these discrepancies to this intrinsic feature of the thermodynamic quantity. For the ranges examined, the convergence between the classical and quantum results observed for other Widom lines (see below) as the range increases is not apparent in this case. This suggests that any such convergence,

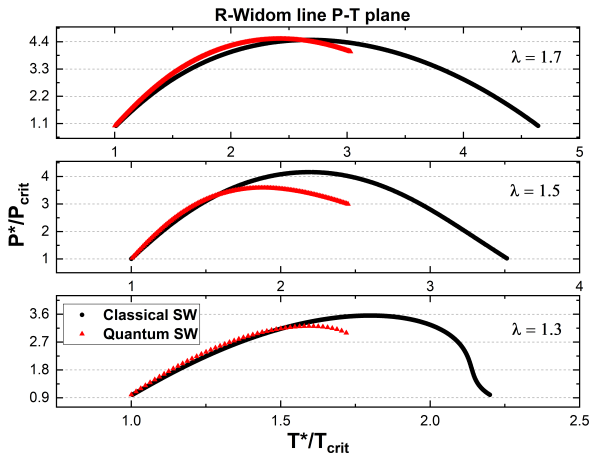


Figure 4: Comparison of the classical and quantum R -Widom lines for $\lambda^* = 1.3$ (bottom), $\lambda^* = 1.5$ (middle), and $\lambda^* = 1.7$ (top).

if present, requires larger ranges outside of the validity domain of the considered EOS.

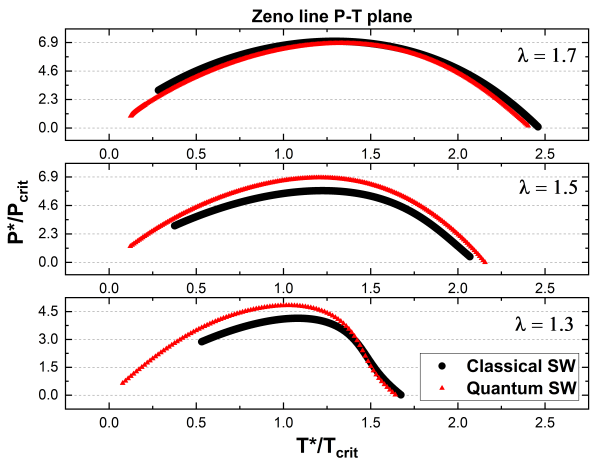


Figure 5: Comparison of the Classical and Quantum Zeno lines for $\lambda^* = 1.3$ (bottom), $\lambda^* = 1.5$ (middle), and $\lambda^* = 1.7$ (upper).

The line often associated in the literature with TG and other geometric formulations of thermodynamics, with the ideal gas behavior [51, 52], was also analyzed. This line is constructed with the set of thermodynamic states with zero curvature, $R^*(T^*, \rho^*) = 0$. For all interaction ranges considered, each of the states that satisfies such condition are located in a very high density region, beyond the domain of validity of the equations of state considered. For this reason, these results are not shown in the present work. Nevertheless, the fact that the same qualitative behavior was observed for all ranges and both classical and quantum fluids suggests that the line $R = 0$, lies in the high-density regime and, therefore, its inter-

pretation as an ideal line in the sense of following an ideal gas-like behavior should be carefully revised and explored.

In the absence of ideal lines emerging from the thermodynamic geometry framework, we explored another well-studied alternative, the Zeno line, defined as the set of thermodynamic states for which the compressibility factor equals one, $Z \equiv P/\rho k_B T$, corresponding to an ideal gas, to enable a comparison, at least qualitatively, of its behavior with that of the ideal line $R = 0$. The result is presented in Fig. 5. The behavior observed for these Zeno lines differs substantially from that of the $R = 0$ lines, and instead resembles the behavior of the Widom lines. In particular, they exhibit a non-monotonic trend: increasing at low temperatures, reaching an extremum, and decreasing at higher temperatures. As in the case of the Widom lines, the discrepancies between classical and quantum results diminish as the interaction range increases and at low temperatures.

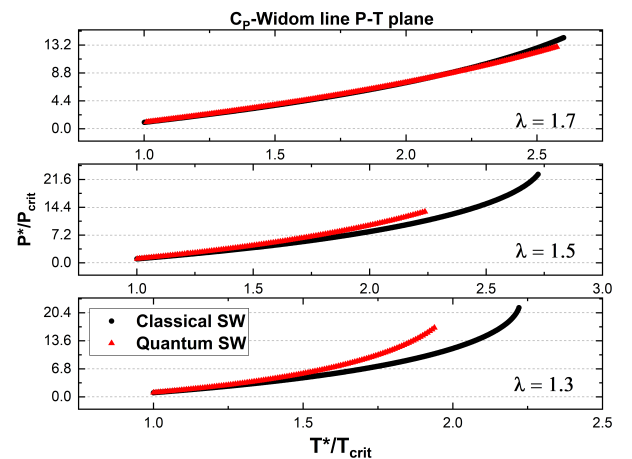


Figure 6: Comparison of the SW Classical and Quantum C_P -Widom lines for $\lambda^* = 1.3$ (bottom), $\lambda^* = 1.5$ (middle), and $\lambda^* = 1.7$ (upper).

As illustrated in Figure 6, the classical and quantum Widom lines, defined by the loci of the maxima of C_p , exhibit distinct behaviors in the different potential ranges considered. Discrepancies are more pronounced for shorter-range interactions; consequently, at a given temperature, the quantum crossover occurs at a pressure higher than that predicted by the classical model, with the difference becoming particularly significant at the shortest ranges.

Similarly, Figure 7 presents the α -Widom lines. As expected, these lines span a region broader than those associated with other response functions or with scalar curvature R . As in previous cases, discrepancies are most pronounced for short-range interactions, with a clear tendency for the classical and quantum results to converge as the range increases.

Interestingly, for the case of the Widom lines associated

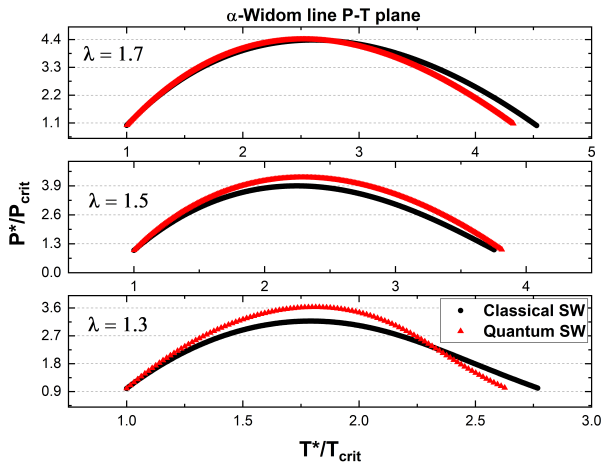


Figure 7: Comparison of the Classical and Quantum α -Widom lines for $\lambda^* = 1.3$ (bottom), $\lambda^* = 1.5$ (middle), and $\lambda^* = 1.7$ (upper).

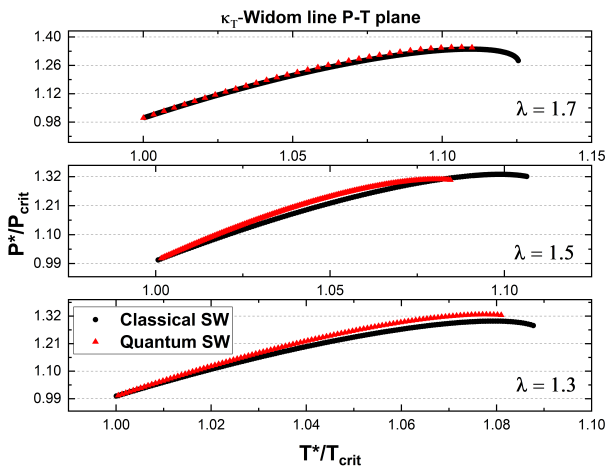


Figure 8: Comparison of the Classical and Quantum κ_T -Widom lines for $\lambda^* = 1.3$ (bottom), $\lambda^* = 1.5$ (middle), and $\lambda^* = 1.7$ (upper).

with the isothermal compressibility, presented in Figure 8, although some differences between the classical and quantum results are evident across the considered ranges, the overall behavior is largely insensitive to both regimes. This suggests that, when accounting for the quantum nature of the fluid, changes in density (related to the compressibility) are less sensitive than changes in temperature (related to the heat capacity and thermal expansion coefficient).

IV. CONCLUSIONS

In this work, we have investigated the impact of quantum contributions on thermodynamic geometry and Widom-line behavior in supercritical fluids within a perturba-

tive framework. By comparing classical and quantum descriptions across multiple interaction ranges, we have assessed how quantum effects modify both geometric and response-function-based indicators beyond the critical point.

Our analysis of the scalar curvature isotherms shows that quantum effects smooth the anomalies typically observed near the critical point and induce a shift of the extrema toward lower densities for short-range potentials. Despite these quantitative changes, the critical behavior itself remains unchanged: the critical exponents are consistent with mean-field predictions for all fluids considered, as expected for a perturbative theory.

The behavior of the R -Widom lines reveals persistent differences between the classical and quantum descriptions across the entire range of interaction ranges examined. Due to the higher-order derivative structure of the scalar curvature R , these discrepancies are plausibly attributable to the intrinsic sensitivity of R to quantum corrections. Unlike other Widom lines, no clear trend toward convergence between classical and quantum results is observed within the explored ranges, suggesting that any such convergence, if present, may only occur for substantially longer interaction ranges, non accessible by the considered quantum SW equation of state.

Thermodynamic lines defined by the condition $R = 0$, often associated with ideal-gas-like behavior, were also examined. For every range considered, these lines were located in a high-density region, outside the validity domain of the equation of state employed. Consequently, a quantitative assessment is not feasible in the current scheme; nevertheless, the consistency of this behavior across all ranges suggests that the interpretation of the $R = 0$ line as a ideal-gas-like behavior should be reconsidered in this context.

For qualitative comparison, the Zeno line, defined by all thermodynamic states that meet the condition $Z = 1$, was analyzed. Its behavior differs markedly from that of the $R = 0$ line, resembling instead that of Widom lines, exhibiting a non-monotonic temperature dependence. As observed for Widom lines, the differences between classical and quantum predictions along the Zeno line decrease with increasing interaction range and at low temperatures.

A systematic comparison of Widom lines associated with different thermodynamic response functions (and scalar curvature) highlights a strong dependence on both the interaction range and the specific thermodynamic quantity considered. Widom lines derived from C_P and from the thermal expansion coefficient α exhibit significant classical–quantum discrepancies for short-range potentials, with a clear tendency towards convergence as the interaction range increases. This feature is in agreement with previous results for the QSW system [10, 24] where quantum effects arising in the HS repulsive term are very relevant, also in the behavior of the perturbation terms, since a_{1P1} significantly differs from the classic value for short-range values of λ^* . In contrast, Widom lines as-

sociated with the isothermal compressibility κ_T , show a relatively minor sensitivity to quantum effects, suggesting that density fluctuations are less affected by quantum corrections than temperature-related fluctuations within the present framework.

Overall, these results suggest that quantum effects can significantly modify thermodynamic features, particularly those associated with thermodynamic geometry, while the universal critical behavior remains unchanged at the current level of approximation. The interplay between interaction range, quantum corrections, and specific thermodynamic observables appears to play a key role in determining the full extent of classical-quantum deviations in bulk systems, motivating further investigation beyond the perturbative regime considered here. The other effect to be considered is the behavior under confinement, where strong effects have been reported previously in connection also with the effective dimension of the system [11, 53, 54].

Acknowledgments

J. L. López-Picón was partially supported by Secretaría

de Ciencia, Humanidades, Tecnología e Innovación (SE-CIHTI) and University of Guanajuato (UG).

L. F. Escamilla-Herrera acknowledge support from SE-CIHTI through postdoctoral grant: Estancias Posdoctorales por México para la Formación y Consolidación de las y los Investigadores por México (CVU: 230753) and UG through grant 401/2025 of Convocatoria Institucional de Investigación Científica 2025.

A. Gil-Villegas acknowledge support from SECIHTI (Grant CBF2023-2024-3350)

J. Torres-Arenas gratefully acknowledges the Departamento de Física Aplicada of the Universidade de Vigo for the facilities and support provided during his sabbatical stay, during which, part of this work was carried out. He also acknowledges the financial support from the Universidad de Guanajuato and SECIHTI (through SNII), which made this stay possible.

-
- [1] S. Kim, D. Henderson, and J. A. Barker, *Canadian Journal of Physics* **47**, 99 (1969), URL <https://doi.org/10.1139/p69-012>.
- [2] S. Nordholm, H. Greberg, and R. Penfold, *Fluid phase equilibria* **90**, 307 (1993).
- [3] B. Yoon and H. A. Scheraga, *The Journal of Chemical Physics* **88**, 3923 (1988), ISSN 0021-9606, URL <https://doi.org/10.1063/1.453841>.
- [4] R. J. Sadus, *The Journal of Physical Chemistry* **96**, 3855 (1992).
- [5] L. M. Sesé and R. Ledesma, *The Journal of Chemical Physics* **102**, 3776 (1995), ISSN 0021-9606, URL <https://doi.org/10.1063/1.468559>.
- [6] D. M. Ceperley, *Rev. Mod. Phys.* **67**, 279 (1995), URL <https://link.aps.org/doi/10.1103/RevModPhys.67.279>.
- [7] Q. Wang and J. Karl Johnson, *Fluid Phase Equilibria* **132**, 93 (1997), ISSN 0378-3812.
- [8] J. P. Wolbach and S. I. Sandler, *Industrial & Engineering Chemistry Research* **36**, 4041 (1997), URL <https://doi.org/10.1021/ie9607255>.
- [9] E. G. Noya, L. M. Sesé, R. Ramírez, C. McBride, M. M. Conde, and C. Vega, *Molecular Physics* **109**, 149 (2011), URL <https://doi.org/10.1080/00268976.2010.528202>.
- [10] V. M. Trejos and A. Gil-Villegas, *The Journal of Chemical Physics* **136**, 184506 (2012).
- [11] V. M. Trejos, A. Gil-Villegas, and A. Martínez, *The Journal of Chemical Physics* **139**, 184505 (2013).
- [12] A. Aasen, M. Hammer, Å. Ervik, E. A. Müller, and Ø. Wilhelmsen, *The Journal of Chemical Physics* **151**, 064508 (2019).
- [13] S. Contreras, A. Martínez-Borquez, C. Avendaño, A. Gil-Villegas, and G. Jackson, *The Journal of Chemical Physics* **160**, 164503 (2024).
- [14] R. Kraemer, A. Mejía, and A. Gil-Villegas, *Journal of Molecular Liquids* **437**, 128249 (2025).
- [15] T. R. Prisk, R. T. Azuah, D. L. Abernathy, G. E. Granroth, T. E. Sherline, P. E. Sokol, J. Hu, and M. Boninsegni, *Phys. Rev. B* **107**, 094511 (2023), URL <https://link.aps.org/doi/10.1103/PhysRevB.107.094511>.
- [16] I. H. Bell, J. W. Leachman, A. F. Rigosi, and H. M. Hill, *Physics of Fluids* **35**, 081703 (2023), ISSN 1070-6631, URL <https://doi.org/10.1063/5.0164037>.
- [17] W. Fang, J. Chen, Y. Feng, X.-Z. Li, and A. Michaelides, *International Reviews in Physical Chemistry* **38**, 35 (2019).
- [18] L. Skrbek, J. J. Niemela, and P. Urban, *Physics of Fluids* **36**, 101303 (2024), ISSN 1070-6631.
- [19] B. Singh and S. Sinha, *Journal of Chemical Physics* **67**, 3645 (1977).
- [20] N. Singh and S. Sinha, *The Journal of Chemical Physics* **69**, 2709 (1978).
- [21] X. Zhao, J. K. Johnson, and C. E. Rasmussen, *The Journal of Chemical Physics* **120**, 8707 (2004), ISSN 0021-9606, URL <https://doi.org/10.1063/1.1695317>.
- [22] H.-Y. Kim, A. D. Lueking, S. M. Gatica, J. K. Johnson, and M. W. Cole, *Molecular Physics* **106**, 1579 (2008).
- [23] I. Georgescu, S. E. Brown, and V. A. Mandelshtam, *The Journal of Chemical Physics* **138**, 134502 (2013), ISSN 0021-9606, URL <https://doi.org/10.1063/1.4796144>.
- [24] C. Serna and A. Gil-Villegas, *Molecular Physics* **114**, 2700 (2016).
- [25] R. Fantoni and S. Moroni, *The Journal of Chemical Physics* **141**, 114110 (2014), ISSN 0021-9606, URL

- <https://doi.org/10.1063/1.4895974>.
- [26] N. Li, X. Wang, N. Gao, and G. Chen, *Physics of Fluids* **37**, 077195 (2025).
- [27] E. Wigner, *Physical review* **40**, 749 (1932).
- [28] J. G. Kirkwood, *Physical Review* **44**, 31 (1933).
- [29] H. S. Green, *The Journal of Chemical Physics* **19**, 955 (1951).
- [30] E. J. Derderian and W. A. Steele, *The Journal of Chemical Physics* **55**, 5795 (1971).
- [31] J. A. Barker, *The Journal of Chemical Physics* **70**, 2914 (1979).
- [32] W. Gibson and S. Byrnes, *Physical Review A* **11**, 270 (1975).
- [33] W. Gibson, *Molecular Physics* **30**, 13 (1975).
- [34] A. Gil-Villegas, A. Galindo, P. J. Whitehead, S. J. Mills, G. Jackson, and A. N. Burgess, *The Journal of Chemical Physics* **106**, 4168 (1997), <https://doi.org/10.1063/1.473101>, URL <https://doi.org/10.1063/1.473101>.
- [35] A. L. Benavides and F. Del Río, *Molecular Physics* **68**, 983 (1989).
- [36] J. Chang and S. I. Sandler, *Molecular Physics* **81**, 745 (1994).
- [37] A. Gil-Villegas, F. del Río, and A. L. Benavides, *Fluid Phase Equilibria* **119**, 97 (1996), ISSN 0378-3812, URL <https://www.sciencedirect.com/science/article/pii/037838129502851X>.
- [38] E. Schöll-Paschinger, A. L. Benavides, and R. Castañeda-Priego, *The Journal of chemical physics* **123** (2005).
- [39] F. del Río, E. Ávalos, R. Espíndola, L. Rull, G. Jackson, and S. Lago, *Molecular Physics* **100**, 2531 (2002), <https://doi.org/10.1080/00268970210132522>, URL <https://doi.org/10.1080/00268970210132522>.
- [40] B. H. Patel, H. Docherty, S. Varga, A. G. *, and G. C. Maitland, *Molecular Physics* **103**, 129 (2005), <https://doi.org/10.1080/00268970412331303990>, URL <https://doi.org/10.1080/00268970412331303990>.
- [41] R. W. Zwanzig, *The Journal of Chemical Physics* **22**, 1420 (1954).
- [42] D. Chandler and P. G. Wolynes, *The Journal of Chemical Physics* **74**, 4078 (1981).
- [43] G. Ruppeiner, *Phys. Rev. A* **20**, 1608 (1979), URL <https://link.aps.org/doi/10.1103/PhysRevA.20.1608>.
- [44] G. Ruppeiner, *Rev. Mod. Phys.* **67**, 605 (1995), URL <https://link.aps.org/doi/10.1103/RevModPhys.67.605>.
- [45] A. Einstein, *Annalen der Physik* **33**, 1275 (1910).
- [46] L. D. Landau and E. M. Lifshitz, *Statistical Physics, Part 1*, vol. 5 of *Course of Theoretical Physics* (Pergamon Press, Oxford, 1980), 3rd ed.
- [47] F. Weinhold, *J. Chem. Phys.* **63**, 2479 ff. (1975).
- [48] N. F. Carnahan and K. E. Starling, *The Journal of Chemical Physics* **51**, 635 (1969).
- [49] A. Gil-Villegas and F. Del Río, *Revista Mexicana de Física* **39** (1993).
- [50] H. Liu, S. Garde, and S. Kumar, *The Journal of chemical physics* **123** (2005).
- [51] H. Quevedo, A. Sánchez, and A. Vázquez, *General Relativity and Gravitation* **47**, 36 (2015), URL <https://doi.org/10.1007/s10714-015-1881-9>.
- [52] H. Quevedo, M. N. Quevedo, and A. Sánchez, *Journal of Geometry and Physics* **176**, 104495 (2022), ISSN 0393-0440.
- [53] S. Contreras and A. Gil-Villegas, *Entropy* **23**, 775 (2021).
- [54] A. Gil-Villegas, K. E. Gubbins, E. E. Santiso, and C. Shang, *The Journal of Chemical Physics* **163**, 244504 (2025).